Lrrk regulates the dynamic profile of dendritic Golgi outposts through the golgin Lava lamp

Chin-Hsien Lin,[1,2*] Hsun Li,[1,3*] Yi-Nan Lee,[1] Ying-Ju Cheng,[1] Ruey-Meei Wu,[2] and Cheng-Ting Chien[1]

[1]Institute of Molecular Biology, Academia Sinica, Taipei 115, Taiwan
[2]Department of Neurology, National Taiwan University Hospital, College of Medicine, National Taiwan University, Taipei 100, Taiwan
[3]Taiwan International Graduate Program in Interdisciplinary Neuroscience, National Yang-Ming University and Academia Sinica, Taipei 115, Taiwan

Constructing the dendritic arbor of neurons requires dynamic movements of Golgi outposts (GOPs), the prominent component in the dendritic secretory pathway. GOPs move toward dendritic ends (anterograde) or cell bodies (retrograde), whereas most of them remain stationary. Here, we show that Leucine-rich repeat kinase (Lrrk), the *Drosophila melanogaster* homologue of Parkinson's disease–associated Lrrk2, regulates GOP dynamics in dendrites. Lrrk localized at stationary GOPs in dendrites and suppressed GOP movement. In *Lrrk* loss-of-function mutants, anterograde movement of GOPs was enhanced, whereas *Lrrk* overexpression increased the pool size of stationary GOPs. Lrrk interacted with the golgin Lava lamp and inhibited the interaction between Lva and dynein heavy chain, thus disrupting the recruitment of dynein to Golgi membranes. Whereas overexpression of kinase-dead Lrrk caused dominant-negative effects on GOP dynamics, overexpression of the human *LRRK2* mutant G2019S with augmented kinase activity promoted retrograde movement. Our study reveals a pathogenic pathway for *LRRK2* mutations causing dendrite degeneration.

Introduction

Neurons are equipped with characteristic patterns of dendritic arbors, which set the framework for neuronal connectivity. Dendrite arborization is regulated by combinatorial codes of transcriptional factors and endomembrane trafficking like endocytosis and exocytosis (Scott and Luo, 2001; Jan and Jan, 2003, 2010; Corty et al., 2009). Local addition and recycling of membrane proteins and lipids are also important for terminal dendrite dynamics such as extension and retraction (Horton and Ehlers, 2004; Hanus and Ehlers, 2008; Yang et al., 2011; Ultanir et al., 2012).

Dendritic Golgi stacks, named Golgi outposts (GOPs), are present as separate entities in shafts, branch points, and terminal branches (Pierce et al., 2001; Horton and Ehlers, 2003; Horton et al., 2005). As the prominent component of the secretory pathway in dendrites, GOPs are required for dendrite growth and maintenance. In pyramidal cells, GOPs primarily localize in apical dendrites that extend most distally, suggesting a correlation between GOPs and dendrite growth. Stationary GOPs locate at branching sites for budding dynamic post-Golgi vesicles (Horton et al., 2005). In *Drosophila melanogaster* class IV dendritic arborization (da) neurons with complex dendritic arbors, growth of dendrites was severely disrupted in mutants of the secretory pathway. Indeed, the local presence of GOPs regulates terminal dendrite dynamics (Ye et al., 2007). Also important are stationary GOPs in terminal branches that serve as sites for acentrosomal microtubule nucleation, promoting microtubule-based dendrite extension and stability (Ori-McKenney et al., 2012).

Unlike axons, in which polarized microtubules are oriented plus end–out uniformly, dendritic microtubules are mixed with both plus and minus end–out microtubules, and the proportions vary in different types of neurons and dendritic segments (Baas and Lin, 2011). In class IV da neurons, microtubules in proximal dendrites are almost minus end–out, whereas both orientations are equally mixed in distal dendrites (Rolls et al., 2007; Stone et al., 2008). The orientation of microtubule polarity regulates distribution and transportation of organelles. GOPs are transported by the dynein complex toward the minus end of microtubules in dendrites. In mutants for dynein components, dendritic GOPs are immobile and localized near cell bodies. Consequently, lower-order dendrites are substituted by higher-order dendrites, resulting in bush-like arbor (Horton et al., 2005; Satoh et al., 2008; Zheng et al., 2008). The Golgi complexes are recruited to the dynein–dynactin complex through the golgin Lava lamp (Lva; Papoulas et al., 2005). Expression of the central coiled-coil domain of Lva causes dominant-negative effects, arresting GOP movements and dendrite growth (Ye et al., 2007). It is still unclear how transportation of GOPs in dendrites is regulated.

*C.-H. Lin and H. Li contributed equally to this paper.

Correspondence to Cheng-Ting Chien: ctchien@gate.sinica.edu.tw

Abbreviations used in this paper: da, dendritic arborization; Dhc, dynein heavy chain; GOP, Golgi outpost; Lrrk, Leucine-rich repeat kinase; Lva, Lava lamp; ManII-GFP, α-mannosidase II–GFP; PD, Parkinson's disease.

© 2015 Lin et al. This article is distributed under the terms of an Attribution–Noncommercial–Share Alike–No Mirror Sites license for the first six months after the publication date (see http://www.rupress.org/terms). After six months it is available under a Creative Commons License (Attribution–Noncommercial–Share Alike 3.0 Unported license, as described at http://creativecommons.org/licenses/by-nc-sa/3.0/).

The Rockefeller University Press $30.00
J. Cell Biol. Vol. 210 No. 3 471–483
www.jcb.org/cgi/doi/10.1083/jcb.201411033

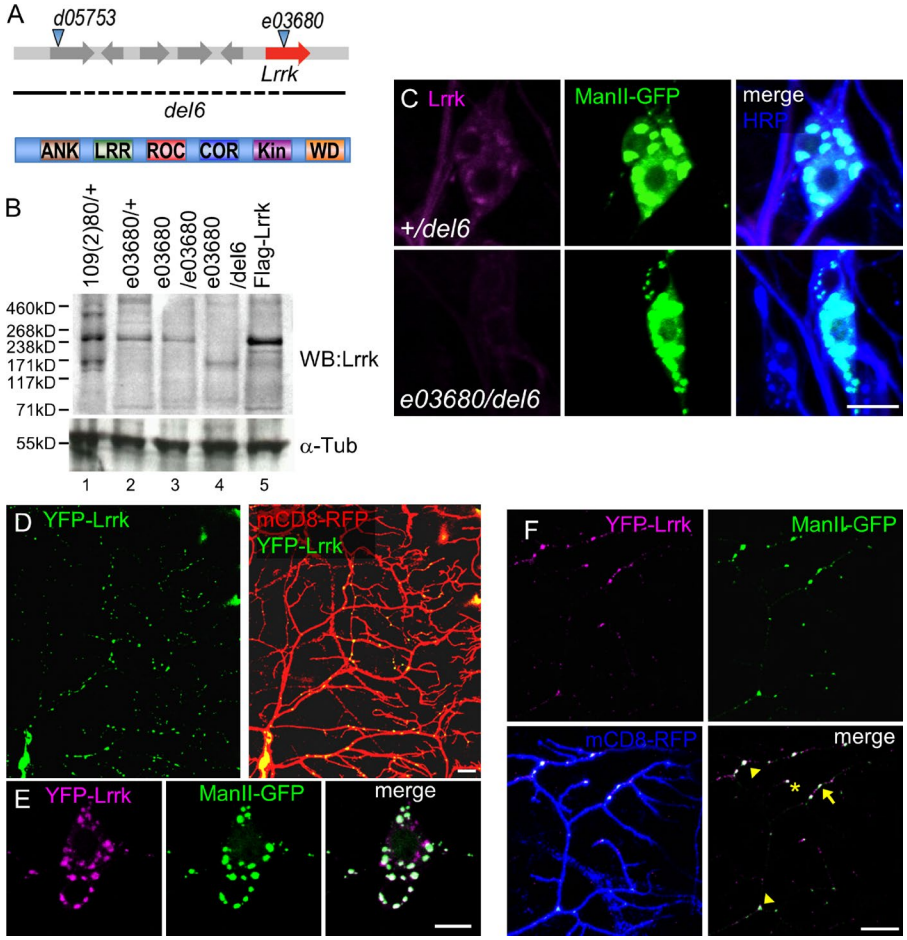

Figure 1. **Lrrk localizes at GOPs in dendrites.** (A) *Lrrk* mutant alleles (top); *e03680* insertion and *del6* allele shown by dashed line. Lrrk domains (bottom): ANK, ankyrin repeats; LRR, leucine-rich repeats; ROC, Ras of complex; COR, C-terminal of ROC; Kin, S/T kinase; and WD, WD40 repeats. (B) Lrrk expressions in different genotypes were detected at 240 kD by Lrrk antibodies and control by α-Tubulin (α-Tub). The experiment was repeated three times. (C) Enriched Lrrk signal (magenta) localizes to ManII-GFP (green) expressed by *ppk-GAL4*. Enriched signal is absent in *e03680/del6* (bottom). HRP is in blue in merged images. (D) Transgenic *YFP-Lrrk* (green) expressed by *ppk-GAL4* shows puncta in mCD8-RFP-labeled neurons (red). (E) Cell bodies show colocalized YFP-Lrrk– (magenta) and ManII-GFP (green)–labeled puncta. (F) Dendrites labeled by mCD8-RFP (blue) show colocalization of YFP-Lrrk (magenta) and ManII-GFP (green). Arrow, arrowhead, and asterisk denote puncta at dendritic shaft, branch point, and tip, respectively. Bars, 10 µm.

Leucine-rich repeat kinase (Lrrk) proteins are members of the ROCO family with a Ser/Thr kinase domain (Lewis, 2009). Lrrk proteins are cytosolic, enriched in the endomembrane system, and implicated in organelle integrity and vesicular trafficking (West et al., 2005; Biskup et al., 2006; Lin et al., 2011). In *Caenorhabditis elegans*, Lrk-1 is required for synaptic vesicle sorting from the somatic Golgi apparatus into axons (Sakaguchi-Nakashima et al., 2007). *Drosophila* Lrrk regulates Rab7-dependent perinuclear localization of lysosomes (Dodson et al., 2012). Human Lrrk2 interacts with ArfGAP1 at Golgi membranes to maintain Golgi integrity (Stafa et al., 2012). Dominant mutations in human *LRRK2* are prevalent in both familial and sporadic Parkinson's disease (PD; Healy et al., 2008; Cookson, 2010). PD mutations of Lrrk2 misroute retromer trafficking to the lysosome instead of the Golgi apparatus (MacLeod et al., 2013). The aforementioned studies support the versatile function of Lrrk proteins in vesicular trafficking. Furthermore, the neuronal levels and activities of Lrrk2 regulate neuronal morphology (MacLeod et al., 2006; Lin et al., 2010). Overexpression of wild-type Lrrk2 induces neurite degeneration, and G2019S mutation with hyperactivated kinase activity (West et al., 2005; Jaleel et al., 2007) further aggravates the defects.

To understand whether Lrrk proteins play a role in regulating vesicular trafficking in neurite morphogenesis, we studied Lrrk in dendrite arborization. By generating the *Lrrk* mutant and YFP-Lrrk transgene, we show that Lrrk localizes at stationary GOPs and regulates GOP dynamics. Through genetic and protein–protein interaction assays, we further suggest that Lrrk antagonizes the interaction between the golgin Lva and dynein heavy chain (Dhc), thus disrupting the minus end–directed transport along microtubules by dynein. Although the kinase activity of Lrrk is required for its function, the gain-of-function *LRRK2* mutation *G2019S* promotes retrograde transport of GOPs toward cell bodies, which correlates with its severe suppressive effect on dendrite arborization.

Results

Lrrk localizes at the Golgi complexes in cell bodies and dendrites

The *Drosophila* genome encodes a single Lrrk orthologue with all conserved functional domains to human Lrrk2 (Fig. 1 A). The Lrrk polypeptide includes 2,351 amino acids and was recognized as an ∼240-kD protein in Western blot analysis (Fig. 1 B, lanes 1 and 2). The signal was enhanced in larvae overexpressing Lrrk via the *UAS-Flag-Lrrk* transgene (Fig. 1 B, lane 5). Substantial expression was still detected in larvae homozygous for the *e03680* insertion (Fig. 1 B, lane 3), which was previously regarded as a strong hypomorphic mutant for *Lrrk* (Lee et al., 2007). We generated the *del6* allele that deleted *Lrrk* (Fig. 1 A). Homozygous mutants for *del6* died in early embryonic stages. However, the trans-heterozygous *del6/e03680* mutant, in which Lrrk expression was largely depleted (Fig. 1 B, lane 4), survived to adult stages, indicating that *del6/e03680* is a strong loss-of-function mutant for *Lrrk*.

Immunohistochemistry using anti-Lrrk antibodies showed that Lrrk expression in larval da neurons was diffusive in cell

bodies, dendrites, and axons, and the expression was markedly reduced in *e03680/del6* mutants (Fig. S1 A). To examine membrane-associated Lrrk, we used detergent-containing fixation buffer that allows permeation of cytosolic fractions but retains membrane-associated components. Using this strategy, we found that Lrrk localized in punctate patterns in cell bodies. Interestingly, these Lrrk-positive puncta colocalized with the α-mannosidase II–GFP (ManII-GFP)–positive Golgi apparatuses (Fig. 1 C). In *e03680/del6* mutants, Lrrk-positive puncta were diminished. Lrrk also colocalized with the CFP-Golgi marker in cell bodies and dendrites at primary branch points and dendritic shafts (Fig. S1 B). Therefore, Lrrk associates with the Golgi complexes in both cell bodies and dendrites.

To better visualize Lrrk localization in dendrites, we generated transgenes for expressing fluorescent protein–tagged Lrrk, YFP-Lrrk, by GAL4 drivers. In da neurons, YFP-Lrrk showed punctate patterns in cell bodies and dendrites, recapitulating the distribution pattern of endogenous Lrrk puncta (Fig. 1 D). These YFP-Lrrk puncta colocalized well with ManII-GFP in cell bodies and dendrites (Fig. 1, E and F). In dendrites, YFP-Lrrk localized mainly at branching points (Fig. 1 F, arrowheads; 39.8 ± 1.7% of total puncta) and shafts (arrow; 56.3 ± 1.7%); localization at dendritic tips was rare (asterisk; 3.9 ± 0.7%). We also examined YFP-Lrrk colocalization with Rab4-mRFP of recycling endosomes, GFP-Rab5 of early endosomes, mCherry-Rab7 of late endosomes, mito-GFP of mitochondria, and GFP-LAMP of lysosomes, which were not as prominent as with ManII-GFP (Fig. S1, C and D). Thus, we focused on Lrrk regulation of the Golgi apparatuses in da neurons.

Lrrk regulates the pool size of stationary GOPs

The majority of GOPs, detected as ManII-GFP puncta, were stationary in da dendrites during the imaging period (Fig. 2, A and B). Dynamic GOPs moved in either anterograde or retrograde direction, and either for a long distance or back and forth within short segments (Fig. 2 C). When examining YFP-Lrrk localization in dendrites, we found that some ManII-GFP–positive puncta were absent of YFP-Lrrk localization. To examine whether YFP-Lrrk–positive puncta were preferentially localized in distinct populations of GOPs, coexpressed ManII-GFP and YFP-Lrrk were imaged simultaneously in living larvae, and puncta were classified into three classes: ManII-GFP and YFP-Lrrk double-positive, ManII-GFP single-positive, and YFP-Lrrk single-positive puncta. We found that double-positive puncta accounted for 57.8 ± 9.0% of total puncta, and 80% of the double-positive puncta were stationary (Fig. 2, A and C [left panels]; and Video 1). In contrast, single ManII-GFP–positive puncta accounted for 37.3 ± 7.3%, and 81% of them were dynamic (Fig. 2 C, right, green arrow). Finally, single YFP-Lrrk–positive puncta accounted for a very small fraction (4.9 ± 5.8%) and almost all of them were stationary (96%). Thus, Lrrk preferentially localizes to stationary GOPs.

The result that YFP-Lrrk–positive puncta were mostly stationary suggests that Lrrk may regulate the pool size of stationary GOPs. We examined the dynamics of GOPs in mutants with reduced Lrrk activity. In *ppk-GAL4* control, 62.9 ± 2.8% of ManII-GFP puncta were stationary (Fig. 2 B). The percentage of stationary puncta showed a significant reduction in *+/del6* (56.7 ± 1.5%), and was further reduced in *e03680/del6* (52.5 ± 3.0%). The reduction of stationary puncta in *e03680/del6* could be restored by the *YFP-Lrrk* transgene (59.1 ± 1.6%),

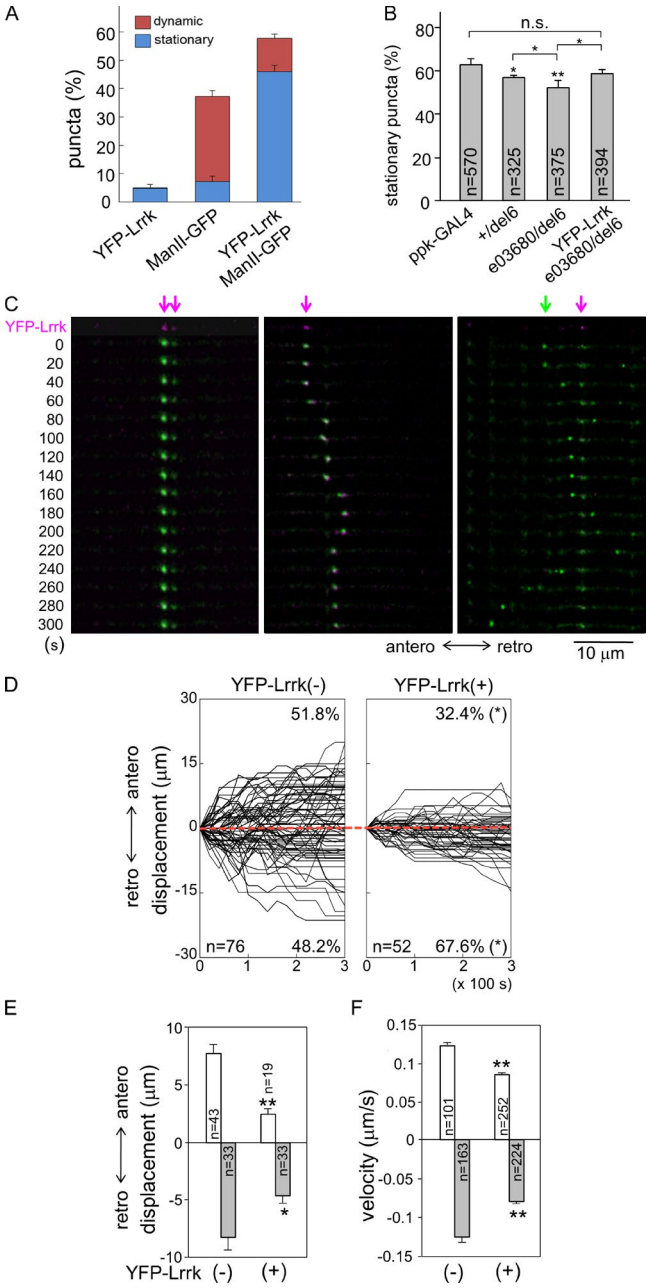

Figure 2. **Lrrk-localized GOPs are stationary.** (A) Bar graph shows percentages of three types of puncta in dendrites, YFP-Lrrk positive, ManII-GFP positive, and double positive driven *ppk-GAL4*, either dynamic (red) or stationary (blue). Mean percentages are from a total 625 puncta of 10 neurons. (B) Bar graph shows percentages of stationary ManII-GFP puncta in genotypes below graph, and statistic significance was compared of *ppk-GAL4* control with total sample numbers from more than five neurons indicated in bars. (C) ManII-GFP puncta (green) with colocalized YFP-Lrrk (magenta arrows) are stationary (left and right columns) or move within a short range (middle). ManII-GFP puncta without YFP-Lrrk (green arrow) travel for long distances (right). The first row shows single YFP-Lrrk signal (magenta) and the rest show merged YFP-Lrrk and ManII-GFP (green) signals. Dendrites were labeled by *ppk-GAL4*-driven mCD8-RFP (not depicted) in third-instar larval stages and straightened for display. Images were taken in 20-s intervals for 5 min. Anterograde (antero) and retrograde (retro) movements are indicated. (D) Tracks of dynamic ManII-GFP puncta without or with YFP-Lrrk colocalization, denoted as YFP-Lrrk(–) and YFP-Lrrk(+), respectively. Punctum numbers and percentages in both directions are indicated within boxes. The x axes represent recording times (seconds) and y axes the displacements of puncta relative to starting points (time 0 and displacement 0). Each track is shown for 5-min recording in 20-s intervals.

which showed no significant difference compared with *ppk-GAL4*. These results suggest that Lrrk regulates the pool size of stationary GOPs in dendrites.

We further analyzed the dynamic behavior of nonstationary ManII-GFP puncta that were positive or negative for YFP-Lrrk, constituting 11.7% or 30.1% of total puncta, respectively (Fig. 2 A). ManII-GFP–positive puncta free of YFP-Lrrk displayed a symmetrical pattern of anterograde and retrograde movements in both percentage and net displacement (Fig. 2, D and E, anterograde [51.8 ± 7.4% and 7.7 ± 0.8 µm] and retrograde [48.2 ± 7.4% and 8.1 ± 1.2 µm]; and Videos 2 and 3). In contrast, double-positive puncta showed asymmetric patterns of movements; more puncta moved in the retrograde direction and they had larger displacements than in the anterograde direction (Fig. 2, D and E, anterograde [32.4 ± 8.9% and 2.5 ± 0.4 µm] and retrograde [67.6 ± 12.1% and 4.6 ± 0.6 µm]; and Videos 4 and 5). Also, both anterograde and retrograde displacements of double-positive puncta were smaller than single ManII-GFP–positive puncta (Fig. 2 E). The difference in the displacements of YFP-Lrrk–free and –localized ManII-GFP puncta could be a result of the difference in the velocities of moving GOPs or the frequency of reversal in anterograde and retrograde directions that nullify the final displacement. We found that YFP-Lrrk–free puncta moved faster in both directions than YFP-Lrrk–localized puncta (Fig. 2 F, YFP-Lrrk–free, anterograde [0.12 ± 0.01] and retrograde [0.13 ± 0.01], and YFP-Lrrk–positive, anterograde [0.09 ± 0.004] and retrograde [0.08 ± 0.003]; unit: µm/s). However, the frequency in reversing the moving direction of GOPs was not affected by Lrrk localization (Fig. S2 A). Thus, GOPs without Lrrk seem to move more freely in both directions. Although most Lrrk-localized GOPs are stationary, the dynamic ones are also less mobile and move preferentially in the retrograde direction.

Lrrk suppresses anterograde movement of GOPs

To examine whether Lrrk restricts GOP movement in dendrites, the directionality and the displacement of dynamic ManII-GFP puncta were further analyzed in *Lrrk* mutants. In *+/del6*, most puncta moved in the retrograde direction (Fig. 3, A [left] and B [anterograde, 32.2 ± 4.6%; and retrograde, 67.8 ± 4.6%]). The displacements in these two directions were also asymmetric, with the retrograde displacement 2.4-fold of the anterograde one (Fig. 3 C, anterograde [5.8 ± 0.8 µm] and retrograde [14.1 ± 1.5 µm in 480 s]), whereas mean velocities of these two directions showed no significant difference (Fig. 3 D, anterograde [0.12 ± 0.006] and retrograde [0.13 ± 0.004 µm/s]). The mean path that averages the displacements of all puncta at each time point indicates that GOPs collectively move in the retrograde direction in *+/del6* (Fig. 3 E, red).

Surprisingly, ManII-GFP puncta in the strong *Lrrk* mutant *e03680/del6* displayed a reverse asymmetry in directionality and displacement. The movement of dynamic ManII-GFP puncta was redirected to the anterograde direction (Fig. 3, A [right] and B [middle; anterograde, 66.3 ± 4.5%; and retrograde, 33.7 ± 4.5%]). Also, compared with *+/del6*, the anterograde displacement had a threefold increase (Fig. 3 C, 17.2 ± 1.9 µm), whereas the retrograde displacement was slightly but not significantly decreased (11.3 ± 2.3 µm). In addition, mean velocities in both anterograde and retrograde directions were increased (Fig. 3 D, anterograde [0.23 ± 0.007] and retrograde [0.20 ± 0.007 µm/s]). The mean path shows that GOPs move collectively in the anterograde direction in *e03680/del6* (Fig. 3 E, black). The reverse in overall directionality and the increased anterograde displacement in the *Lrrk* mutant indicate that Lrrk mainly suppresses GOP movements toward the distal end of dendrites. Indeed, the distribution of GOPs was shifted distally in *e03680/del6* compared with *+/del6*, whereas the number of GOPs remained not significantly different (Fig. S2, B and C). Thus, the distribution of GOPs correlates with the change of GOP dynamics in the *Lrrk* mutant.

We then examined whether the enhanced anterograde movement of GOPs in *e03680/del6* is caused by the lack of Lrrk activity. In *e03680/del6* carrying the *YFP-Lrrk* transgene, the preferred directionality of GOPs was restored to retrograde (Fig. 3 B, right, 74.8 ± 5.7%) and the anterograde displacement was suppressed, showing no significant difference to *+/del6* (Fig. 3 C, 4.7 ± 0.9 µm). The mean velocities in anterograde and retrograde directions were also suppressed to close to controls (Fig. 3 D, anterograde [0.14 ± 0.004] and retrograde [0.16 ± 0.004 µm/s]). The mean path shows that ManII-GFP puncta move collectively in the retrograde direction (Fig. 3 E, blue). Thus, Lrrk functions in class IV da neurons to inhibit anterograde movement of GOPs in dendrites.

Lrrk suppresses dendrite arborization

Dynamic movements and distributions of GOPs correlate with terminal dendrite behaviors such as extension and retraction, resulting in modulation of overall dendrite morphology (Ye et al., 2007). With the regulation of GOP dynamics by Lrrk, we addressed whether YFP-Lrrk localization regulates dendrite growth. Terminal dendrites with or without YFP-Lrrk puncta at branching sites, denoted as YFP-Lrrk(−) and YFP-Lrrk(+), respectively, were assayed for their dynamic behaviors (Fig. 4 A). We found that YFP-Lrrk(−) dendrites extended with a larger displacement and more frequently than YFP-Lrrk(+) dendrites (Fig. 4 C). In addition, YFP-Lrrk(+) dendrites were stalled more often. These differences result in positive displacement of YFP-Lrrk(−) terminal dendrites. We also assayed how terminal dendrite dynamics are affected by the lack of *Lrrk* through recording their extension and retraction (Fig. 4 B). Terminal dendrites of *e03680/del6*, as compared with *+/del6*, showed no significant difference in the displacement of extension or retraction (Fig. 4 D), but were more frequent in extension and less frequent in retraction, contributing to an increase in net displacement.

We then assayed the impact of Lrrk in dendrite arborization patterns. In *e03680/del6* neurons lacking *Lrrk* activity, the dendritic pattern was more complex, with increased terminal branches (Fig. 4, E and G). The increase in dendrites was also found in complex class IV da neurons of *e03680/del6* (Fig. 4, F and H). However, the dendrites of simple class I da neurons were normal in *Lrrk* mutants (Fig. S3, A and B), suggesting that Lrrk activity regulates higher-order dendrite

Anterograde displacement is shown as plus and retrograde as minus. Red dotted lines are aligned along displacement 0. (E and F) Bar graphs show mean anterograde and retrograde displacements (E) and velocities (F) for YFP-Lrrk(−) and YFP-Lrrk(+), with statistic significance compared between two groups. Error bars represent SEM. Statistical comparisons are to controls (unless specifically indicated) by Student's *t* test. *, $P < 0.05$; **, $P < 0.001$; n.s., no significance.

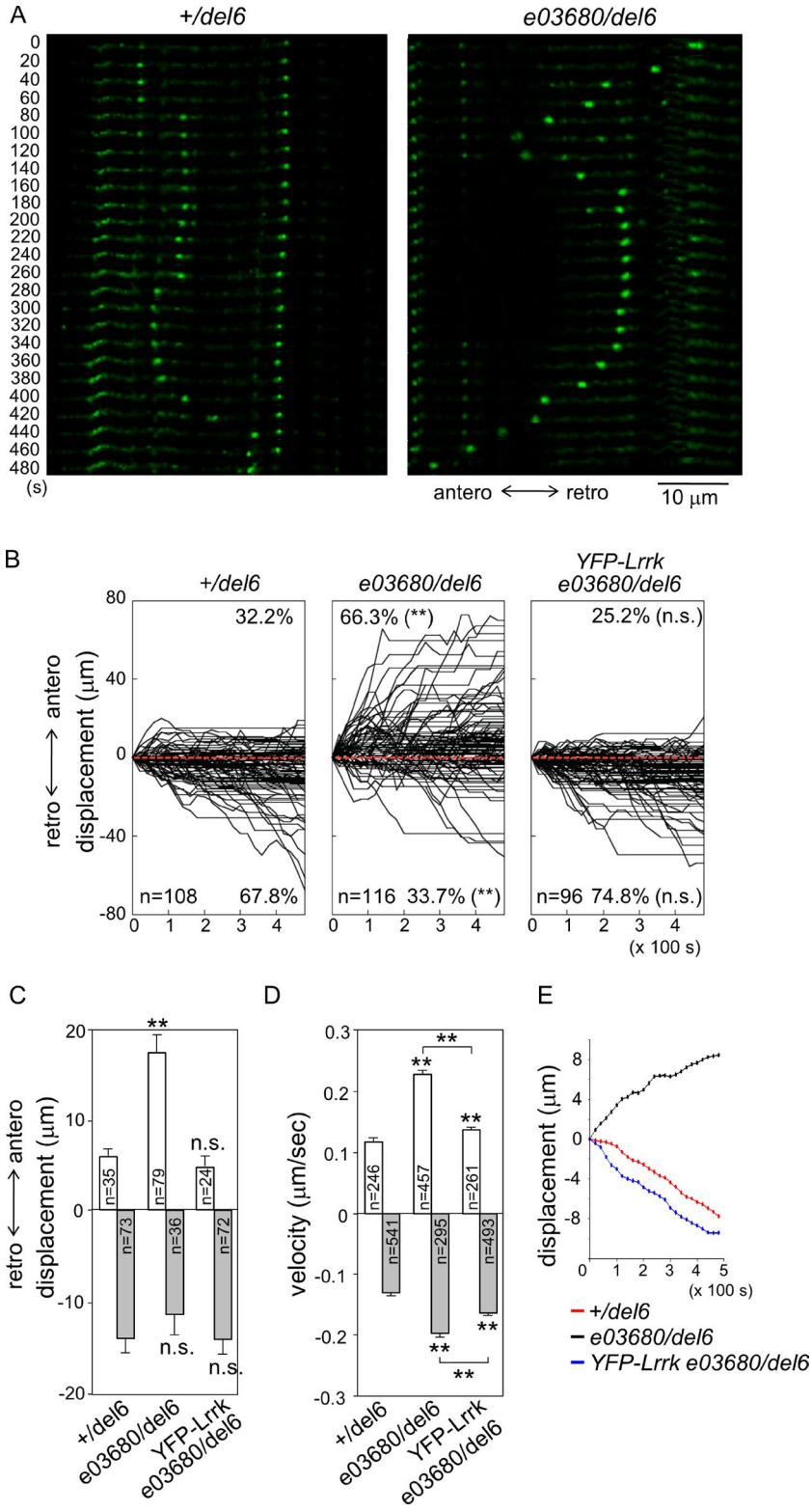

Figure 3. **Lrrk suppresses GOP anterograde movement.** (A) Movement of ManII-GFP puncta expressed by *ppk-GAL4* in *+/del6* (left) and *e03680/del6* (right). Image series were taken for 8 min in 20-s intervals in dendrites of third-instar larvae and are shown, as done for Fig. 2 C. (B) Combined tracks of ManII-GFP puncta are shown for an 8-min period with 20-s intervals for genotypes shown above each panel. (C and D) Bar graphs show mean displacements (C) and velocities (D) of puncta. Error bars represent SEM. Statistical comparisons are to controls (unless specifically indicated) by Student's *t* test. *, $P < 0.05$; **, $P < 0.001$; n.s., no significance. (E) Mean paths show average displacements of puncta at every time point for the three genotypes.

arborization. Sholl analysis of dendrite distribution suggests the increases of dendrites in medial and distal ranges (Fig. S3 C). Finally, we addressed whether the increase in dendrites is caused by the lack of Lrrk activity. Overelaboration of dendrites in *e03680/del6* was suppressed by neuronal expression of YFP-Lrrk (Fig. 4 G). These analyses indicate that Lrrk is required cell autonomously in neurons to suppress dendrite arborization.

Lrrk antagonizes the interaction between Lva and Dhc

The golgin Lva recruits the Golgi apparatus to the dynein–dynactin complex for minus end–directed transportation along microtubules (Papoulas et al., 2005). We tested whether Lrrk interacts with Lva to regulate dendrite arborization. S2 cells were transfected with *Flag-Lrrk* or *Flag-GFP*, and the Flag immunoprecipitates were examined for the presence of Lva by

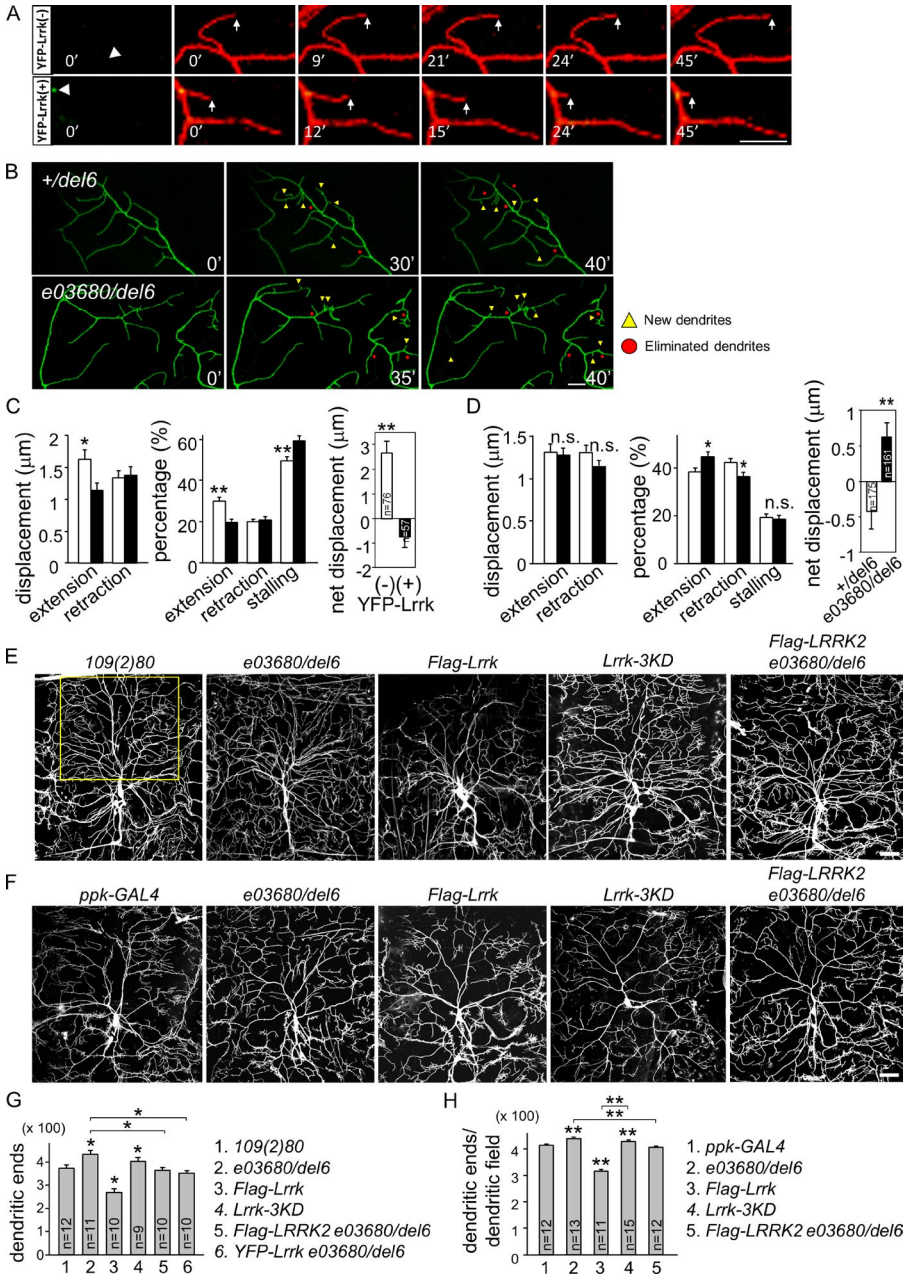

Figure 4. **Lrrk suppresses dendrite development.** (A) Time series of images (3-min interval in 45 min) show terminal dendrites labeled by *ppk-GAL4*-driven mCD8-RFP (red) for YFP-Lrrk(–) and YFP-Lrrk(+) (green). Arrowheads indicate dendritic bases and arrows indicate dynamic terminal dendrites. (B) Images of terminal dendrites labeled by *ppk-GAL4*-driven mCD8-GFP for *+/del6* and *e03680/del6* at 0 min, at 40 min, and at an intermediate stage. Yellow triangles, new dendrites; red dots, eliminated dendrites. Bars, 10 µm. (C) Bar graphs show quantifications for dendrite dynamics in A, with YFP-Lrrk(–) as open bars and YFP-Lrrk(+) as shaded bars, with displacements in 3-min intervals in extension (1.63 ± 0.15 and 1.34 ± 0.10 µm, respectively) and retraction (1.14 ± 0.11 and 1.37 ± 0.13 µm); percentages in extension (30.2 ± 1.7 and 19.6 ± 2.4%), retraction (20.2 ± 2.1 and 20.9 ± 2.1%), and stalling (49.6 ± 2.2 and 59.4 ± 2.7%); and net displacements (2.66 ± 0.49 and –0.75 ± 0.43 µm) after 45-min recording. (D) Bar graphs show terminal dendrites of *+/del6* (open bar) and *e03680/del6* (shaded bar) for displacements in extension (1.32 ± 0.09 and 1.29 ± 0.07 µm) and retraction (1.31 ± 0.08 and 1.16 ± 0.06 µm); percentages in extension (38.3 ± 1.8 and 44.8 ± 1.8%), retraction (42.4 ± 1.7 and 36.6 ± 1.6%), and stalling (19.3 ± 1.5 and 18.6 ± 1.4%); and net displacements (–0.42 ± 0.25 and 0.66 ± 0.21 µm) in 40 min. (E and F) Images of da dendrites labeled by *109(2)80*-driven (E) or *ppk-GAL4*-driven (F) mCD8-GFP with genotypes indicated on top. Bars, 50 µm. (G and H) Bar graph shows mean dendritic ends in the upper part of dorsal fields (outlined by yellow rectangle in E). (G) *109(2)80* (380.6 ± 18.4), *e03680/del6* (446.2 ± 19.7), *Flag-Lrrk* (280.3 ± 17.1), *Lrrk-3KD* (402.1 ± 19.3), *Flag-LRRK2 e03680/del6* (362.1 ± 17.2), and *YFP-Lrrk e03680/del6* (342.1 ± 16.8). (H) *ppk-GAL4* (413.3 ± 12.2), *e03680/del6* (439.5 ± 17.5), *Flag-Lrrk* (317.5 ± 19.3), *Lrrk-3KD* (429.9 ± 16.6), and *Flag-Lrrk2 e03680/del6* (408.6 ± 15.8). Error bars represent SEM. Statistical comparisons are to controls (unless specifically indicated) by Student's *t* test. *, $P < 0.05$; **, $P < 0.001$; n.s., no significance.

Western blot analysis (Fig. 5 A). Consistent with an interaction between Lrrk and Lva, Lva signal was detected in Flag-Lrrk but not Flag-GFP immunoprecipitates. The interaction between Lrrk and Lva was further confirmed by coimmunoprecipitation in brain extracts of transgenic flies expressing Flag-Lrrk by pan-neuronal *elav-GAL4* (Fig. 5 B).

Lva links Golgi membranes to the dynein–dynactin–based microtubule transport system. The central coiled-coil domain Lva3 interacts with $p150^{Glued}$ of the dynactin complex, and the C-terminal globular domain Lva5 interacts with both $p150^{Glued}$ and Dhc (Papoulas et al., 2005). To map the Lva-interacting domains with Lrrk, Myc-tagged Lva domains (1, 2A, 2B, 2C, 3, 4, and 5) were tested individually in S2 cells for coimmunoprecipitation by Flag-Lrrk. Lva3 and Lva5 were detected in Western blots analyzed by Myc antibodies, suggesting that both Lva3 and Lva5 interact with Lrrk (Fig. 5 C).

The Lrrk interactions with Lva3 and Lva5 might modulate the interactions of Lva to dynein and dynactin components. To test this, GST-fused Lva3 and Lva5 were used to pull down Lrrk from adult head lysates expressing different gene dosages of *Lrrk*. In lysates prepared from wild type or *elav-GAL4*, GST-Lva3 but not GST-Lva1 control pulled-down $p150^{Glued}$, confirming the interaction between Lva3 and the dynactin component. The interaction between Lva3 and $p150^{Glued}$ in controls was compared with *+/del6*, *e03680/e03680*, and *e03680/del6* that express reduced Lrrk levels and to *UAS-Flag-Lrrk* overexpression that increases Lrrk levels. However, the interaction remained constant regardless of different Lrrk levels (Fig. 5 D). We then tested the interaction between Lva5 and Dhc in wild type and *Lrrk* mutants and overexpression. Again, we confirmed that GST-Lva5 was able to interact with Dhc in controls (Fig. 5 E). Interestingly, the pulled-down Dhc level was dramatically reduced when Lrrk was overexpressed and was

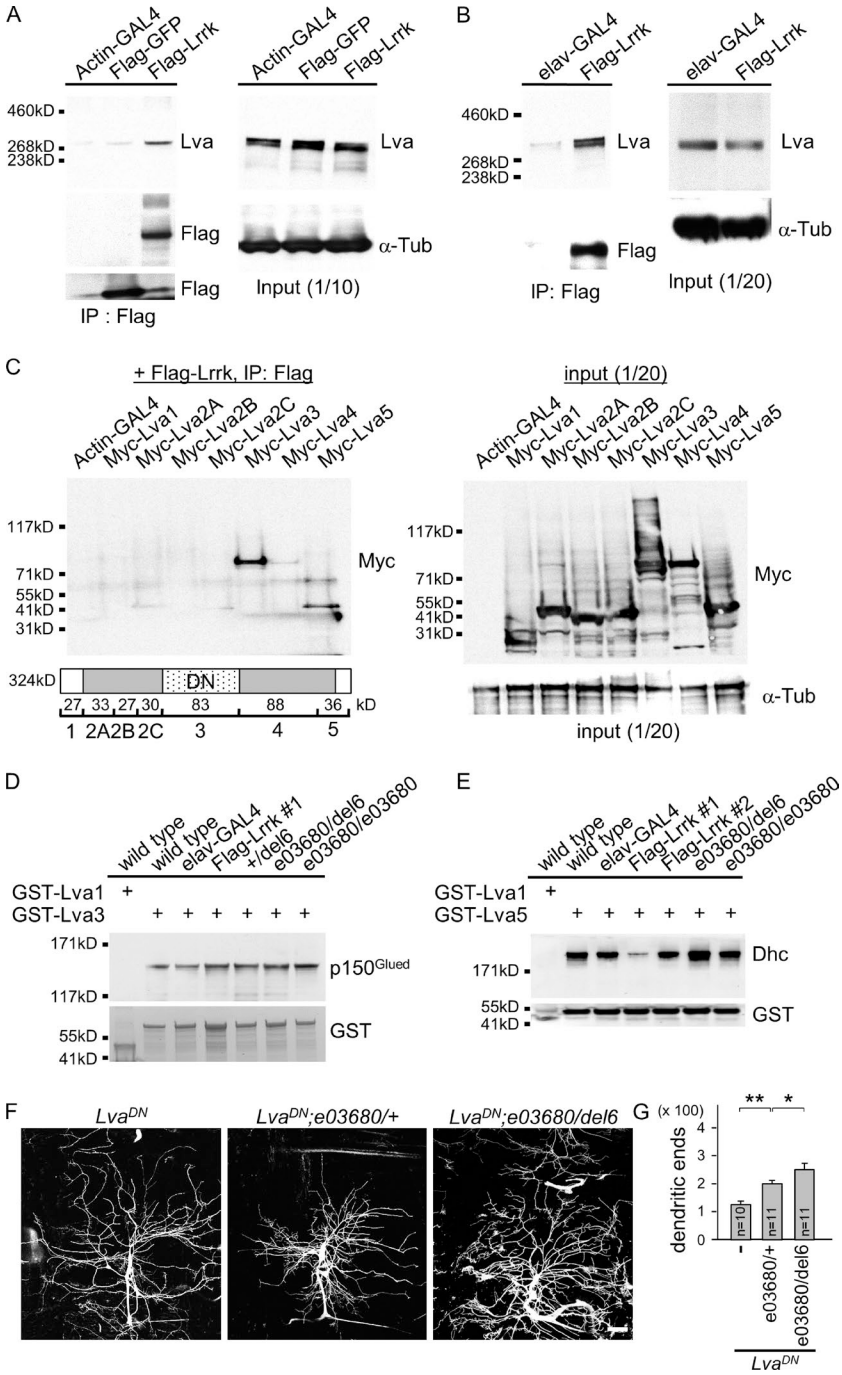

Figure 5. **Lrrk antagonizes the interaction between Lva and Dhc.** (A and B) Western blots show coimmunoprecipitated Lva in Flag immunoprecipitates from S2 cells transfected with *UAS-Flag-Lrrk* or *UAS-Flag-GFP* driven by *Actin-GAL4* (A) or from adult head extracts prepared from *elav-GAL4* or *elav-GAL4 Flag-Lrrk* flies (B). The Flag immunoprecipitates were probed with antibodies for Lva and Flag (left) and input controls with Lva or α-Tub antibodies (right). (C) Western blot by Myc antibodies shows Myc-Lva3 and Myc-Lva5 were detected in Flag immunoprecipitates (left) from S2 cells transfected with *Flag-Lrrk* and one of Myc-tagged Lva domains (bottom, cartoon). Expressions of Lva domains by *Actin-GAL4* were detected by Myc antibodies and input control by α-Tub antibodies (right). Cartoon shows Lva domains and predicted molecular masses; and Lva^{DN} corresponds roughly to Lva3. (D and E) Western blots show pulled-down $p150^{Glued}$ by GST-Lva3 (D) and Dhc by GST-Lva5 (E) in adult brain extracts prepared from wild type (w^{1118}), *elav-GAL4* control, *Flag-Lrrk* overexpression (#1 and #2), *+/del6*, *e03680/del6*, and *e03680/e03680*. Flag-Lrrk #1 is a strong while #2 is a weak expression line. The amounts of GST-Lva3 and GST-Lva5 and negative control GST-Lva1 are shown in bottom panels. Experiments in A–E were repeated three times. (F) Images of da dendrites labeled by *109(2)80*-driven mCD8-GFP with genotypes indicated on top. (G) Bar graph shows mean dendritic ends as done for Fig. 4 E for Lva^{DN} (115.2 ± 8.9), Lva^{DN}; *e03680/+* (191.5 ± 10.3), and Lva^{DN}; *e03680/del6* (223.4 ± 23.1). Error bars represent SEM. Statistical comparisons are to controls (unless specifically indicated) by Student's *t* test. *, $P < 0.05$; **, $P < 0.001$; n.s., no significance.

enhanced in the *Lrrk* mutant *e03680/del6* (Fig. 5 E). Collectively, these results strongly suggest that Lrrk competes with Dhc for interaction with Lva5.

Expression of the dominant-negative form of Lva, Lva^{DN}, in da neurons caused dendrite reduction and field shrinkage (Fig. 5, F and G; Ye et al., 2007). Sholl analysis indicates that dendrites of Lva^{DN} neurons decrease in medial and distal regions and slightly increase in proximal regions (Fig. S3 D). To test whether suppression of dendrite arborization by Lva^{DN} is mediated through Lrrk, *Lrrk* mutant alleles were introduced into Lva^{DN}-expressing neurons. The single *e03680* allele increased the number of Lva^{DN} dendrites (Fig. 5, F and G), in particular in proximal and medial ranges (Fig. S3 D). Further reduction of Lrrk activity in the *e03680/del6* mutant increased even more dendrites in Lva^{DN} (Fig. 5, F and G), mainly in medial and long ranges (Fig. S3 D). The restoration of dendrite arborization defects by reducing *Lrrk* gene dosages suggests that Lrrk is required for Lva^{DN} to inhibit dendrite arborization.

Lrrk kinase activity is required in regulating GOP dynamics and dendrite arborization

We next examined whether Lrrk overexpression has an impact on the dynamic profile of GOPs in dendrites. In da neurons with Flag-Lrrk overexpression by *ppk-GAL4*, the percentage of stationary ManII-GFP puncta was increased significantly (Fig. 6 A, *ppk-GAL4* [62.9 ± 2.8%] and *Flag-Lrrk* [76.9 ± 2.5%]). The percentage of GOPs moving toward the retrograde direction was also enhanced, from 58.7 ± 7.7% in *ppk-*

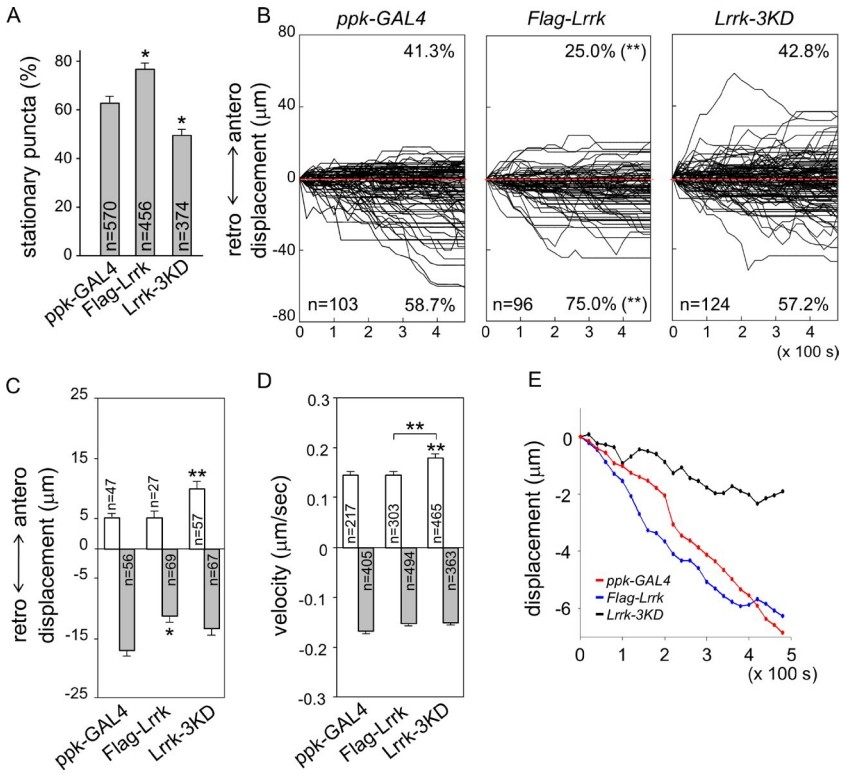

Figure 6. **Requirement of kinase activity for Lrrk function.** (A) Bar graph shows percentages of stationary ManII-GFP puncta for *ppk-GAL4*, *Flag-Lrrk*, and *Lrrk-3KD* overexpression from more than five neurons. (B) Combined tracks of dynamic ManII-GFP puncta are shown as done for Fig. 3 B. (C and D) Bar graphs show mean anterograde and retrograde displacements after 8-min recording (C) and velocities (D). Error bars represent SEM. Statistical comparisons are to controls (unless specifically indicated) by Student's *t* test. *, $P < 0.05$; **, $P < 0.001$; n.s., no significance. (E) Mean paths of ManII-GFP movement for the three genotypes.

GAL4 to 75.0 ± 5.7% in *Flag-Lrrk* (Fig. 6 B). Overexpression of Lrrk also suppressed the retrograde displacement (Fig. 6 C, *ppk-GAL4* [17.0 ± 1.8 μm] and *Flag-Lrrk* [11.4 ± 1.2 μm]) without affecting the basal anterograde displacement (*ppk-GAL4* [5.2 ± 0.6 μm] and *Flag-Lrrk* [5.4 ± 1.0 μm]). Mean velocities in anterograde and retrograde movements remained almost identical to control (Fig. 6 D, anterograde and retrograde for *ppk-GAL4* [0.15 ± 0.006 and 0.17 ± 0.006] and *Flag-Lrrk* [0.15 ± 0.006 and 0.15 ± 0.005 μm/s]). The mean path of ManII-GFP puncta indicates that Lrrk overexpression leads to enhancement of retrograde movement (Fig. 6 E). The distribution of GOPs in dendrites was also shifted toward the proximal region (Fig. S2 C). Thus, overexpression of Lrrk increases the pool size of stationary GOPs and enhances retrograde movement of mobile GOPs.

To test the involvement of Lrrk kinase activity in regulating GOP dynamics, Lrrk-3KD with ablated kinase activity (Imai et al., 2008) was overexpressed by *ppk-GAL4*. In contrast to overexpression of Flag-Lrrk, Lrrk-3KD significantly reduced the percentage of stationary puncta (Fig. 6 A, 50.0 ± 2.2%). Thus, Lrrk-3KD functions dominant-negatively in regulating the pool size of stationary GOPs. Although overexpression of Flag-Lrrk promoted retrograde movements, Lrrk-3KD had no such effect (Fig. 6 B, right, retrograde: *ppk-GAL4* [58.7 ± 7.7%] and *Lrrk-3KD* [57.2 ± 5.0%]). Instead, anterograde puncta in *Lrrk-3KD* overexpression moved further (Fig. 6 C, 9.9 ± 1.3 μm), with a twofold increase of the *ppk-GAL4* control (5.2 ± 0.6 μm) and *Flag-Lrrk* overexpression (5.4 ± 1.0 μm). The retrograde displacement showed no significant difference to *ppk-GAL4* and *Flag-Lrrk* (Fig. 6 C, *Lrrk-3KD* [13.5 ± 1.9 μm]). The increase in anterograde displacement was contributed from the enhanced anterograde velocity (Fig. 6 D, 0.18 ± 0.006 μm/s), whereas there was no difference in retrograde velocity (0.15 ± 0.004 μm/s). The mean path of puncta in Lrrk-3KD overexpression suggests that GOPs move in the retrograde direction at much reduced rates (Fig. 6 E). Also in contrast to the Flag-Lrrk overexpression, Lrrk-3KD overexpression promotes more distal distribution of GOPs in dendrites (Fig. S2 C).

We then examined whether the Lrrk kinase activity plays a role in dendrite development. Overexpression of Lrrk in da neurons suppressed dendrite arborization, causing significant reduction in terminal dendrites and dendritic fields (Fig. 4, E and G). However, overexpression of Lrrk-3KD abolished the suppression and slightly induced dendrite overgrowth. The effect of overexpression of Flag-Lrrk was mainly on higher order dendrites, as concluded from examining dendrite phenotypes of class IV and I da neurons (Fig. 4, F and H; and Fig. S3, A and B). Also, Lrrk-3KD overexpression induced overgrowth of class IV dendrites. Collectively, these results suggest that inactivation of the kinase activity either abolishes the effects of Lrrk overexpression or causes dominant-negative effects on GOP movements and dendrite development.

The kinase activity of Lrrk is required to antagonize the Lva–Dhc interaction

With the requirement of Lrrk kinase activity on GOP dynamics and dendrite arborization, we tested whether inactivation of the Lrrk kinase affects the interaction between Lva5 and Dhc. In the GST pull-down assay, the interaction between Lva5 and Dhc was consistently suppressed by Flag-Lrrk overexpression (Fig. 7 A, second and third lanes). Interestingly, higher levels of Dhc were detected in Lrrk-3KD overexpression than in Flag-Lrrk overexpression (Fig. 7 A, fourth lane). Although the level of Lva5-associated Dhc was increased in Lrrk-3KD overexpression, the level of Lrrk that was bound to Lva5 was comparable to that in Flag-Lrrk overexpression (Fig. 7 B, third and fourth lanes). Thus, kinase-inactivated Lrrk was still capable of binding to Lva5, but failed to suppress the interaction between Lva5 and

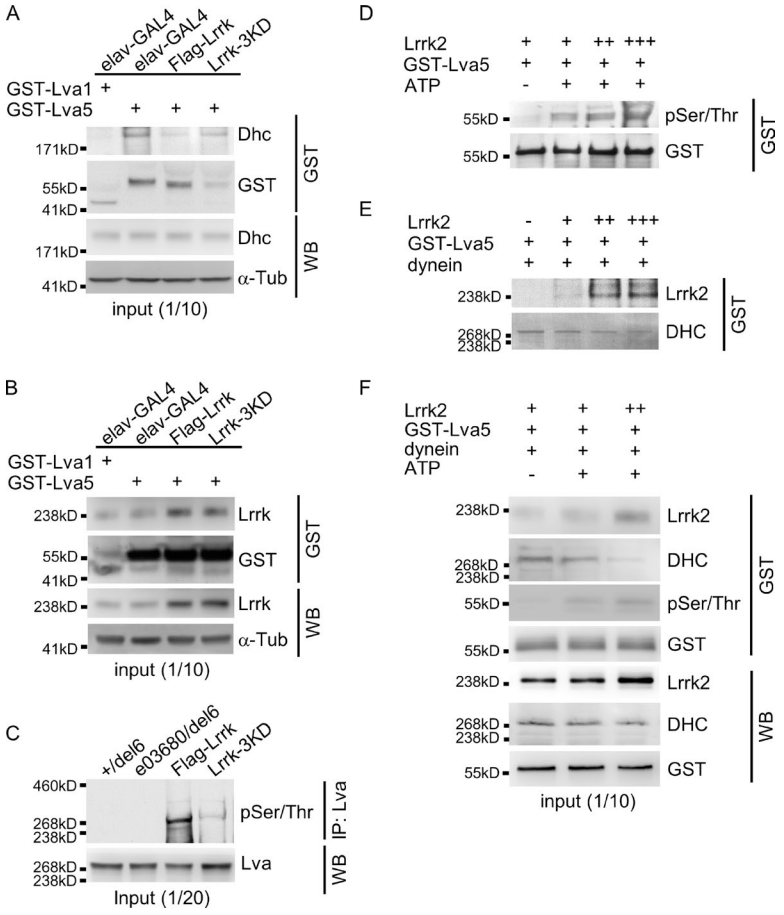

Figure 7. **Kinase activity of Lrrk proteins in Lva phosphorylation and Dhc interaction.** (A and B) Western blots show pulled-down Dhc (A) or Lrrk (B) by GST-Lva5 or GST-Lva1 from fly head extracts of *elav-GAL4* control and *Flag-Lrrk* or *Lrrk-3KD* overexpression. GST as pull-down controls and α-Tub as input controls. (C) Western blot shows pSer/Thr of Lva in Lva immunoprecipitates for *+/del6*, *e03680/del6*, and *Flag-Lrrk* or *Lrrk-3KD* overexpression by *elav-GAL4*. (D–F) Western blots show coprecipitated pSer/Thr and GST (D), Lrrk2 and DHC (E) or Lrrk2, DHC, pSer/Thr, and GST (F) in GST pull-down complexes from incubations of Lrrk2 with GST-Lva5 (D) or with GST-Lva5 and dynein (E and F) with or without 10 mM ATP followed by GST pull-down. Input control was analyzed by antibodies for Lrrk2, DHC, and GST (F). Experiments were all performed three times except once for C because of a limited amount of Lva antibodies.

Dhc, suggesting that the kinase activity of Lrrk is the primary factor to antagonize the interaction between Lva5 and Dhc.

To examine the effect of Lrrk on Lva phosphorylation, Lva was immunoprecipitated by anti-Lva antibodies, and serine and threonine phosphorylation (pSer/Thr) was examined in Western blots probed by the MPM2 antibody (Logarinho and Sunkel, 1998). In *+/del6* and *e03680/del6*, phosphorylation of Lva was not prominent. However, immunoprecipitated Lva was phosphorylated when Flag-Lrrk was overexpressed, and the phosphorylation was greatly reduced by Lrrk-3KD overexpression (Fig. 7 C). Therefore, Lrrk is involved in the phosphorylation of Lva in vivo.

To test for a direct phosphorylation of Lva by Lrrk, we used the purified human Lrrk2 protein. With increasing amounts of Lrrk2 incubated with equal amounts of GST-Lva5, increasing levels of pSer/Thr were detected for the pulled-down Lva5 (Fig. 7 D). Almost no phosphorylation was detected in the absence of ATP (Fig. 7 D, first lane). As Lrrk2 was coprecipitated with the pulled-down GST-Lva5 (Fig. 7 E), these results strongly suggest that Lrrk2 can directly bind and phosphorylate Lva5.

To test the competition between Lrrk2 and human DHC to bind to Lva5, the purified dynein complex was incubated with Lrrk2 and GST-Lva5, and GST-Lva5 was pulled down. In the absence of Lrrk2, DHC was detected in the pulled-down complex. However, with more input of Lrrk2, the levels of Lrrk2 in GST pull-down also increased, and the levels of precipitated DHC decreased (Fig. 7 E). Indeed, increases in Ser/Thr phosphorylation of GST-Lva5 correlate with decreases in the amount of GST-Lva5–bound DHC (Fig. 7 F). Collectively, these results strongly support the idea that Lrrk2 binds to and phosphorylates Lva5, and phosphorylated Lva5 failed to interact with the dynein component Dhc.

Lrrk2 G2019S mutation enhances retrograde transport of GOPs

Overexpression of human Lrrk2 proteins, either wild type or disease mutants, induce dendrite degeneration, with the hyperactive mutant G2019S causing the most severe phenotype (Lin et al., 2010). G2019S-K1906M with inactivation of the hyperactivity also causes dendrite degeneration, although to a lesser extent. The effects of Lrrk on GOP dynamics in dendrites prompted us to examine how human Lrrk2 proteins affect GOP dynamics in dendrites. We first showed that human Lrrk2 could functionally substitute for *Drosophila* Lrrk, as Lrrk2 suppressed dendrite overgrowth in the *Lrrk* mutant *e03680/del6* (Fig. 4, E–H). Also, Lrrk2 interacted with Lva5 and antagonized the interaction between Lva5 and DHC (Fig. 7, D–F). Overexpression of Lrrk2 in class IV da neurons displayed the same preference of retrograde movement as in *ppk-GAL4* control (Fig. 8 A, 61.7 ± 6.24%, compared with 58.7 ± 7.7% in *ppk-GAL4* in Fig. 6 B). Whereas anterograde displacement was slightly increased (*ppk-GAL4*, 5.2 ± 0.6 µm, and *LRRK2*, 6.1 ± 0.8 µm; $P < 0.05$ by Students' *t* test), the retrograde displacement was suppressed (*ppk-GAL4*, 17.0 ± 1.8 µm, and *LRRK2*, 10.56 ± 1.0 µm; $P < 0.01$). Thus, similar to *Drosophila* Lrrk, Lrrk2 functions in suppressing retrograde movement. In comparison to Lrrk2, both G2019S and G2019S-K1906M reversed the suppression, showing larger retrograde displacements (Fig. 8 B, *G2019S* [17.9 ± 1.56 µm] and *G2019S-K1906M* [17.1 ± 2.2 µm]) and higher percentages of puncta in retrograde direction (Fig. 7 A, *G2019S* [75.9 ± 4.5%]

and *G2019S-K1906M* [66.0 ± 6.3%]). Both mutants also induced significantly anterograde displacements (*G2019S* [9.7 ± 1.2 µm] and *G2019S-K1906M* [8.8 ± 1.2 µm]). Mean velocities of GOP movements were also increased, which was more prominent in *G2019S* in both anterograde and retrograde, with larger velocity in retrograde than anterograde (Fig. 8 C, anterograde and retrograde in µm/s: *LRRK2*, 0.14 ± 0.005 and 0.14 ± 0.003; *G2019S*, 0.19 ± 0.009 and 0.23 ± 0.006; and *G2019S-K1906M*, 0.16 ± 0.008 and 0.17 ± 0.005). Therefore, the specific G2019S mutation promotes GOP retrograde movement by enhancing frequency, velocity, and displacement of retrograde movement, and inactivation of kinase activity suppresses the changes in directionality and velocities of GOPs to different extents. Finally, we assayed the mean paths of puncta and showed that both G2019S and G2019S-K1906M mutants induced further retrograde movements of GOPs toward the cell bodies (Fig. 8 D). Collectively, the PD mutation G2019S induces profoundly retrograde movements of GOPs, consistent with its prominent role in causing dendrite reduction and shrinkage.

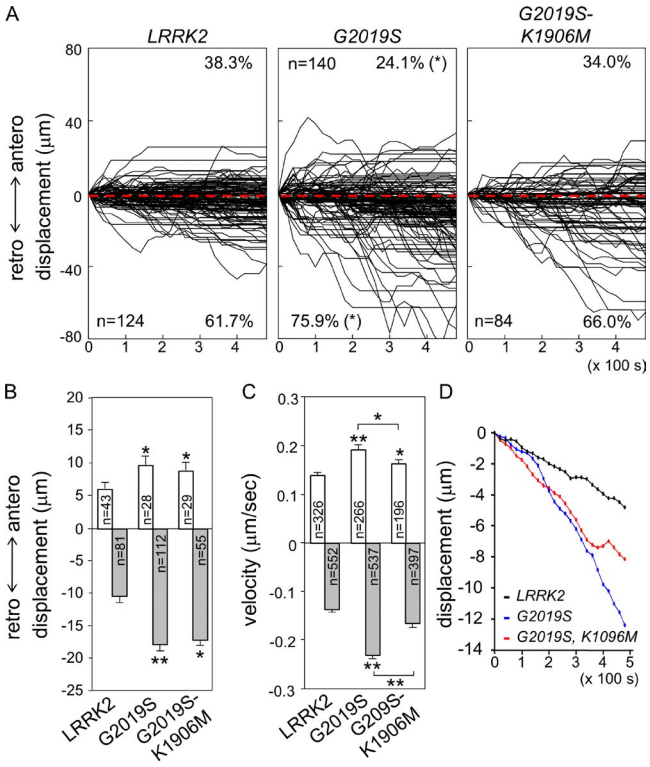

Figure 8. **Impacts of human LRRK2 proteins on GOP dynamics.** (A) Combined tracks of ManII-GFP puncta are shown for *ppk-GAL4* overexpression of *LRRK2*, *G2019S*, and *G2019S-K1906M*. (B and C) Bar graphs show anterograde and retrograde displacements in 8 min (B) and mean anterograde and retrograde velocities. Error bars represent SEM. Statistical comparisons are to controls (unless specifically indicated) by Student's *t* test. *, P < 0.05; **, P < 0.001; n.s., no significance. (D) Mean paths of ManII-GFP puncta in these three overexpressions.

Discussion

Here we show that Lrrk regulates the dynamic profile of dendritic GOPs, and the results could justify the role of Lrrk on dendrite arborization. In dendrites, Lrrk localizes to GOPs and inhibits GOP movements, thus increasing the pool of stationary GOPs (see the model in Fig. 9). Further analysis of mobile GOPs indicates that Lrrk preferentially suppresses anterograde movement of GOPs, a process likely dependent on dynein-based transport on minus end–out microtubules. The genetic and biochemical analyses suggest that Lrrk interacts with the golgin Lva that tethers GOPs to the minus end–directed dynein complex. Lrrk binding to the Lva5 domain suppresses the association of Lva to Dhc, thus unloading GOPs from the dynein-based transport system. The kinase activity of Lrrk is required to antagonize the Lva–Dhc interaction and to regulate GOP movement and dendrite arborization. Interestingly, the dominant mutation G2019S of LRRK2 promotes GOP retrograde movement. This regulation of GOP dynamics is consistent with the role of G2019S in suppressing dendrite arborization.

GOPs are wildly distributed and highly mobile in neurons with complex dendritic patterns (Horton and Ehlers, 2003; Ye et al., 2007). GOPs regulate local dendrite growth and stability, which could be mediated via its conventional role in membrane addition and protein transportation (Hanus and Ehlers, 2008). By regulating GOP dynamics, Lrrk could play a prominent role in shaping the dendrite arborization pattern. Lrrk inhibits GOP dynamics, in particular in anterograde movement. In *Lrrk* loss-of-function mutants, more GOPs display motility toward distal dendritic ends. Indeed, many GOPs moved processively in the

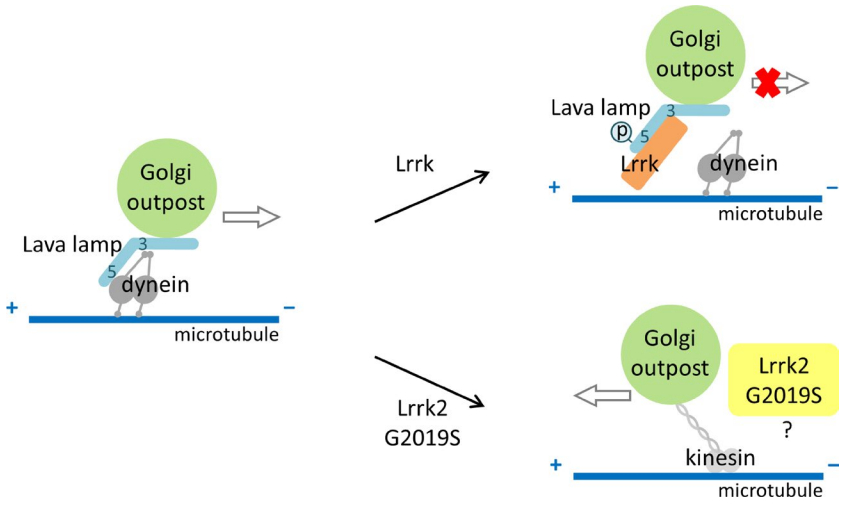

Figure 9. **Model for Lrrk regulation of GOP dynamics.** In the absence of Lrrk, GOPs are transported by dynein toward minus ends of microtubules (left). Lrrk binds to and phosphorylates Lva, disrupting the association of GOPs to dynein, leaving GOPs static (top right). Lrrk2 mutation G2019S promotes GOP movement toward cell bodies, a process that might rely on kinesin-based transport (bottom right).

anterograde direction without disruption, traveling for a long distance (Fig. 3 B). The enhanced anterograde movement depends on the dynein–dynactin complex, which was abolished in RNAi knockdown of Dhc and p150^{Glued} (Fig. S4). This enhancement of anterograde movement could make more GOPs available in higher-order dendrites for further elaboration. In contrast, overexpression of Lrrk inhibits anterograde transport and increases the population of stationary GOPs in dendrites. Overexpression of Lrrk also inhibits the retrograde transport to a lesser extent (Fig. 6 C). The inhibition of retrograde movement could be a result of the smaller fraction of plus end–out microtubules that also mediates dynein–dynactin–based transport toward cell bodies. Indeed, RNAi knockdown for Dhc and p150^{Glued} showed retarded GOP movements in both anterograde and retrograde directions (Fig. S4). By disrupting the association between the golgin Lva and Dhc, Lrrk inhibition of GOP movement could be mediated by a step in dislodging GOPs from the dynein transport system, thus increasing the static population, which could be also available for transport by plus end–directed motors. Although more GOPs were mobile in *Lrrk* mutants, ∼50% of GOPs still maintained static (Fig. 2 B). This group of Lrrk-insensitive GOPs might consist of distinct functional populations, such as for microtubule nucleation (Ori-McKenney et al., 2012; Zhou et al., 2014) and post-Golgi vesicle budding (Horton et al., 2005). We suggest that the fraction of Lrrk-halted GOPs is poised for conversion to mobile ones by dynein-based transport along microtubules, thus providing an immediate response to growth signals.

Golgi-associated golgin proteins contain long stretches of coiled-coil domains, forming long parallel homodimers, and recruit cytoplasmic interacting proteins through C-terminal regions (Barr and Short, 2003; Munro, 2011). The interaction of golgins to the dynein–dynactin complexes has significant roles in Golgi organization, trafficking, and positioning (Hoogenraad et al., 2001, 2003; Matanis et al., 2002; Yadav et al., 2012). Lva, proposed to be the homologue of Giantin (Munro, 2011), mediates apical movement of the Golgi complexes during cellularization in early embryos (Papoulas et al., 2005). Lva is also required for GOP localization and transportation in dendrites (Ye et al., 2007). Our study provides a mechanistic view on how Lrrk regulates GOP dynamics in dendrites. Direct binding of the Golgi adaptor Lva to dynein allows transport of GOPs in dendrites. This interaction is antagonized by Lrrk that would abolish the recruitment of dynein to the golgin Lva and hence the transport of GOPs toward the minus end of microtubules. Lrrk could phosphorylate at Ser/Thr sites of Lva through direct protein–protein interaction. Although kinase-inactivated Lrrk was still capable of interacting with Lva, it failed to antagonize the Lva–Dhc interaction, which could explain the dominant-negative effect of Lrrk-3KD in GOP dynamics and dendrite arborization.

Dysfunctional Golgi complexes have been linked to neurodegenerative diseases, including PD (Fan et al., 2008). PD is characterized by insoluble fibrillar aggregates of α-synuclein in both soma and neurites (Goedert, 2001). Interestingly, the cellular toxicity caused by α-synuclein overexpression could be suppressed by the small GTPase Rab1 that regulates ER-to-Golgi vesicular transport (Chua and Tang, 2006; Cooper et al., 2006). Our study shows that human Lrrk2, similar to *Drosophila* Lrrk, suppressed GOP retrograde movements. Interestingly, the G2019S variant with enhanced kinase activity instead facilitates retrograde movement. Thus, the G2019S mutation may redirect GOP movement toward the plus end of microtubules to cell bodies. It has been shown that kinesin 1 is also required in dendrite arborization, and mutants for kinesin heavy chain displayed bushy dendrite morphology that is identical to dynein mutants (Satoh et al., 2008). Further studies exploring how hyperactivated G2019S promotes the transport toward the plus end of microtubules is needed. Our findings emphasize the significance of GOP regulation by Lrrk proteins, which might be a contributing factor in PD.

Materials and methods

Drosophila strains, transgenic lines, and plasmid construction

GAL4 lines used in this study were *elav-GAL4* for expression in all neurons, *109(2)80* for expression in all classes of da neurons, and *ppk-GAL4* for expression in class IV da neurons. Stocks bearing transgenes with the UAS regulatory sequence were *UAS-Flag-Lrrk* (described below for plasmid construction); *UAS-YFP-Lrrk* (described below); *UAS-Lrrk3KD* with triple mutations K1781M, D1882A, and D1912A in the kinase domain (Imai et al., 2008); *UAS-LRRK2*; *UAS-LRRK2-G2019S*; *UAS-LRRK2-G2019S-K1906M* for expression of human Lrrk2 wild-type and mutant proteins (Lin et al., 2010); *UAS-mC-D8GFP* for membrane-tethered GFP; *UAS-ManII-GFP* for the Golgi-resident enzyme ManII-GFP (Ye et al., 2007; a gift from Y.N. Jan, University of California, San Francisco, San Francisco, CA); *UAS-Lva^{DN}* for expressing the central coiled-coil Lva3 region (amino acids Glu1122 to Ala1800; Fig. 5 C, bottom; Ye et al., 2007; a gift from Y.N. Jan); *UAS-CFP-Golgi* for expressing CFP tagged with a Golgi targeting signal (Satoh et al., 2008); *UAS-mCherry-Rab7* for marking late endosomes (a gift from J.C. Hsu, National Tsing-Hua University, Hsinchu, Taiwan); *UAS-Rab4-mRFP* for marking recycling endosomes (Bloomington Drosophila Stock Center [BDSC]); *UAS-GFP-Rab5* for marking early endosomes (BDSC); *UAS-mito-GFP* for marking mitochondria (BDSC); and *UAS-GFP-LAMP* for marking lysosomes (Pulipparacharuvil et al., 2005; a gift from C.K. Yao, Institute of Biological Chemistry, Academia Sinica, Taipei, Taiwan). RNAi transgenes of *UAS-Dhc64C^{RNAi}* (28054; Vienna Drosophila Resource Center) and *UAS-Glued^{RNAi}* (3785; Vienna Drosophila Resource Center) were for knockdown of Dhc of dynein and the p150Glued subunit of dynactin, respectively. Fly strains carrying mutant alleles are *PBac[RB]Lrrk^{e03680}* and *del6* that is derived from the FRT-mediated intra-chromosomal recombination between two *piggy-BAC* insertion lines (*e03680* and *d05753*). The full-length *Lrrk* coding region was amplified by RT-PCR from an adult cDNA library and cloned into *pENTR/D-TOPO* (Invitrogen) to generate the entry clone, which was recombined with the destination vector *pPFMW* carrying N-terminal 3xFLAG (Drosophila Gateway Vector Collection). *UAS-YFP-Lrrk* was generated by subcloning the full-length *Lrrk* cDNA into the N terminus tagged *pUAST-Venus* vector (Drosophila Genomics Resource Center).

Live imaging of GOPs and image acquisition and processing

Live imaging was conducted with modification of a previously described procedure (Yang et al., 2011). Early third-instar larvae were mounted with double-sided tape between two coverslips to be incorporated into an imaging chamber for anesthetization with a short pulse of desflurane (Suprane; Boxter) that sedates larvae for 10 min (Füger et al., 2007). Immersol W (Carl Zeiss) fills between coverslip and lens for imaging at room temperature. Images were acquired via confocal microscope (LSM710 inverted; Carl Zeiss) under a 40× objective lens (NA 1.2, C-Apochromat 40×/1.2 W Corr M27; Carl Zeiss) through the software Zen 2010 (Carl Zeiss). Series of images for ManII-GFP in

distal dendritic regions of class IV da neurons were taken with 20-s intervals within 8–10 min. Dynamic ManII-GFP puncta in consecutive images were tracked down by the segmented line tool, and punctum displacement was quantified by ImageJ (version 1.48; National Institutes of Health). In a given field of successive images, ManII-GFP puncta that moved <0.3 µm were considered as stationary ones. Videos of ManII-GFP and YFP-Lrrk were generated by the straighten tool in ImageJ for presentation. YFP-Lrrk and other subcellular compartments such as Rab4-mRFP, GFP-Rab5, mCherry-Rab7, GFP-LAMP, or mito-GFP puncta in da neurons of anesthetized third-instar larvae were imaged with the same mounting procedure and imaging setup. Live imaging of mCD8-GFP–marked dendrites and YFP-Lrrk puncta in awakening third-instar larvae was performed by confocal microscopy (LSM710) with an image captured every 3 to 5 min. Data analysis and statistics were performed via Excel (Microsoft), SigmaPlot (ver. 11.0; Systat Software Inc.), and Matlab (MathWorks) software.

Immunostaining and image acquisition and processing

Primary antibodies used in the study were for Flag (mouse; Sigma-Aldrich), GFP (mouse; Invitrogen), Myc (rabbit; Santa Cruz Biotechnology, Inc.), α-Tubulin (mouse; Sigma-Aldrich), HRP-conjugated Cy5 (rabbit; Jackson ImmunoResearch Laboratories, Inc.), phospho-Ser/Thr-Pro (MPM-2, mouse; EMD Millipore), GST (mouse; Sigma-Aldrich), and Lva (rabbit; Papoulas et al., 2005; a gift from J.C. Sisson, University of Texas at Austin, Austin, TX). The antibody for *Drosophila* Lrrk was generated in rabbits against the peptide sequence of amino acids 172–191 (LYQTY-RDEEG-QWEWR-LPF-DAC; BioSource) and titrated 1:300 for immunostaining and 1:1,000 for immunoblotting. Secondary antibodies used were anti–rabbit Cy3 (donkey) and anti–mouse Alexa Fluor 488 (goat) from Jackson ImmunoResearch Laboratories, Inc.

Dissected third-instar larvae were fixed with 4% paraformaldehyde (and 0.5% Triton X-100 for membrane permeation in Fig. 1 C), and were then blocked in 5% normal donkey serum in PBT. After immunostaining, filleted larvae were mounted in 87% glycerol solution for imaging under 20× objective (NA 0.75, Fluar 20×/0.75; Carl Zeiss) with a confocal microscope (LSM 510; Carl Zeiss). Images were acquired via LSM 510 META and processed via LSM 5 Image Examiner (Carl Zeiss).

Immunoprecipitation, GST pull-down assay, and Western blotting

Drosophila S2 cells were maintained in serum-free medium at 25°C. 2×10^5 S2 cells in 24-well dishes were transfected with 200 ng DNA of individual constructs using Effectene (QIAGEN). Transfection of S2 cell and immunopurification of FLAG protein from the transfected cell lysate and Western blot analysis were performed as described previously (Lin et al., 2010). For preparation of fly head extracts, 50–60 fly heads were collected and homogenized in 500 µl of RIPA buffer (50 mM Tris-HCl, pH 8.0, with 150 mM sodium chloride, 1.0% Igepal CA-630 [NP-40], 0.5% sodium deoxycholate, and 0.1% sodium dodecyl sulfate) with proteinase inhibitors (Roche). The extracts were further subjected to centrifugation at 15,000 rpm at 4°C for 15 min, and the supernatants were used for immunoprecipitation or Western blot analysis. Protein concentrations were determined by protein assay (Bio-Rad Laboratories).

For immunoprecipitations, antibodies were prebound to Affi-Gel protein A beads (Bio-Rad Laboratories) and the bound antibody–bead complexes were washed three times and equilibrated in extraction buffer. The prebound antibody−beads were then incubated with S2 cell lysates or fly head extracts (2 mg of total protein) for 2 h before further analysis by Western blots. In the GST pull-down assay, GST fusion proteins (10–20 µg) bound to GST beads were incubated with the lysates at 4°C overnight. Immunoprecipitated or GST pulled-down pellets were subjected to electrophoresis in 3–8% Tris-acetate gradient SDS-NuPAGE (Invitrogen) and then transferred to nitrocellulose membrane for immunoblotting.

For protein–protein interaction in Fig. 7 (D–F), LRRK2 protein (+, 0.15 µg; ++, 0.5 µg; and +++, 1.5 µg; Life Technologies), GST-purified GST-Lva1 or GST-Lva5 (10–20 µg), and cytoplasmic dynein motor protein (2 µg; Cytoskeleton, Inc.) with or without 10 mM ATP were used.

Online supplemental material

Fig. S1 describes Lrrk expression and colocalization with Golgi or other organelle markers in da neurons. Fig. S2 shows the reversal of movement, number, and distribution of GOPs in dendrites in genotypes with different *Lrrk* gene dosages. Fig. S3 shows no effects on class I dendrites by different *Lrrk* gene dosages and Sholl analysis of dendrites in all classes of da neurons affected by *Lrrk* gene dosages and Lva^{DN}. Fig. S4 shows the effects of expressing Dhc^{RNAi} and $Glued^{RNAi}$ in class IV da neurons on GOP dynamics. Videos 1–5 display the movement of GOPs with or without YFP-Lrrk colocalization in dendrites. Online supplemental material is available at http://www.jcb.org/cgi/content/full/jcb.201411033/DC1.

Acknowledgments

We thank J.C. Sisson (died on 27 October 2009) for anti-Lva antibody and pGEX-Lva clones; Y.N. Jan, J.C. Hsu, and C.K. Yao for fly stocks; Y.H. Wang and M.L. Huang for analyzing dynein phenotypes; S.Y. Huang for advice on statistics; S.P. Lee of the Institute of Molecular Biology (IMB) imaging core for imaging assistance; members of the IMB Fly Food Kitchen and FlyCore in Taiwan for assistance; and members of the Chien laboratory for discussion and comments.

This work is supported by grants from the Ministry of Science and Technology and Academia Sinica.

The authors declare no competing financial interests.

Submitted: 11 November 2014
Accepted: 16 June 2015

References

Baas, P.W., and S. Lin. 2011. Hooks and comets: The story of microtubule polarity orientation in the neuron. *Dev. Neurobiol.* 71:403–418. http://dx.doi.org/10.1002/dneu.20818

Barr, F.A., and B. Short. 2003. Golgins in the structure and dynamics of the Golgi apparatus. *Curr. Opin. Cell Biol.* 15:405–413. http://dx.doi.org/10.1016/S0955-0674(03)00054-1

Biskup, S., D.J. Moore, F. Celsi, S. Higashi, A.B. West, S.A. Andrabi, K. Kurkinen, S.W. Yu, J.M. Savitt, H.J. Waldvogel, et al. 2006. Localization of LRRK2 to membranous and vesicular structures in mammalian brain. *Ann. Neurol.* 60:557–569. http://dx.doi.org/10.1002/ana.21019

Chua, C.E., and B.L. Tang. 2006. α-Synuclein and Parkinson's disease: the first roadblock. *J. Cell. Mol. Med.* 10:837–846. http://dx.doi.org/10.1111/j.1582-4934.2006.tb00528.x

Cookson, M.R. 2010. The role of leucine-rich repeat kinase 2 (LRRK2) in Parkinson's disease. *Nat. Rev. Neurosci.* 11:791–797. http://dx.doi.org/10.1038/nrn2935

Cooper, A.A., A.D. Gitler, A. Cashikar, C.M. Haynes, K.J. Hill, B. Bhullar, K. Liu, K. Xu, K.E. Strathearn, F. Liu, et al. 2006. α-Synuclein blocks ER-Golgi traffic and Rab1 rescues neuron loss in Parkinson's models. *Science.* 313:324–328. http://dx.doi.org/10.1126/science.1129462

Corty, M.M., B.J. Matthews, and W.B. Grueber. 2009. Molecules and mechanisms of dendrite development in *Drosophila*. *Development.* 136:1049–1061. http://dx.doi.org/10.1242/dev.014423

Dodson, M.W., T. Zhang, C. Jiang, S. Chen, and M. Guo. 2012. Roles of the *Drosophila* LRRK2 homolog in Rab7-dependent lysosomal positioning. *Hum. Mol. Genet.* 21:1350–1363. http://dx.doi.org/10.1093/hmg/ddr573

Fan, J., Z. Hu, L. Zeng, W. Lu, X. Tang, J. Zhang, and T. Li. 2008. Golgi apparatus and neurodegenerative diseases. *Int. J. Dev. Neurosci.* 26:523–534. http://dx.doi.org/10.1016/j.ijdevneu.2008.05.006

Füger, P., L.B. Behrends, S. Mertel, S.J. Sigrist, and T.M. Rasse. 2007. Live imaging of synapse development and measuring protein dynamics using two-color fluorescence recovery after photo-bleaching at *Drosophila* synapses. *Nat. Protoc.* 2:3285–3298. http://dx.doi.org/10.1038/nprot.2007.472

Goedert, M. 2001. α-Synuclein and neurodegenerative diseases. *Nat. Rev. Neurosci.* 2:492–501. http://dx.doi.org/10.1038/35081564

Hanus, C., and M.D. Ehlers. 2008. Secretory outposts for the local processing of membrane cargo in neuronal dendrites. *Traffic.* 9:1437–1445. http://dx.doi.org/10.1111/j.1600-0854.2008.00775.x

Healy, D.G., M. Falchi, S.S. O'Sullivan, V. Bonifati, A. Durr, S. Bressman, A. Brice, J. Aasly, C.P. Zabetian, S. Goldwurm, et al. 2008. Phenotype, genotype, and worldwide genetic penetrance of LRRK2-associated Parkinson's disease: a case-control study. *Lancet Neurol.* 7:583–590.

Hoogenraad, C.C., A. Akhmanova, S.A. Howell, B.R. Dortland, C.I. De Zeeuw, R. Willemsen, P. Visser, F. Grosveld, and N. Galjart. 2001. Mammalian Golgi-associated Bicaudal-D2 functions in the dynein–dynactin pathway by interacting with these complexes. *EMBO J.* 20:4041–4054. http://dx.doi.org/10.1093/emboj/20.15.4041

Hoogenraad, C.C., P. Wulf, N. Schiefermeier, T. Stepanova, N. Galjart, J.V. Small, F. Grosveld, C.I. de Zeeuw, and A. Akhmanova. 2003. Bicaudal D induces selective dynein-mediated microtubule minus end-directed transport. *EMBO J.* 22:6004–6015. http://dx.doi.org/10.1093/emboj/cdg592

Horton, A.C., and M.D. Ehlers. 2003. Dual modes of endoplasmic reticulum-to-Golgi transport in dendrites revealed by live-cell imaging. *J. Neurosci.* 23:6188–6199.

Horton, A.C., and M.D. Ehlers. 2004. Secretory trafficking in neuronal dendrites. *Nat. Cell Biol.* 6:585–591. http://dx.doi.org/10.1038/ncb0704-585

Horton, A.C., B. Rácz, E.E. Monson, A.L. Lin, R.J. Weinberg, and M.D. Ehlers. 2005. Polarized secretory trafficking directs cargo for asymmetric dendrite growth and morphogenesis. *Neuron.* 48:757–771. http://dx.doi.org/10.1016/j.neuron.2005.11.005

Imai, Y., S. Gehrke, H.Q. Wang, R. Takahashi, K. Hasegawa, E. Oota, and B. Lu. 2008. Phosphorylation of 4E-BP by LRRK2 affects the maintenance of dopaminergic neurons in *Drosophila*. *EMBO J.* 27:2432–2443. http://dx.doi.org/10.1038/emboj.2008.163

Jaleel, M., R.J. Nichols, M. Deak, D.G. Campbell, F. Gillardon, A. Knebel, and D.R. Alessi. 2007. LRRK2 phosphorylates moesin at threonine-558: characterization of how Parkinson's disease mutants affect kinase activity. *Biochem. J.* 405:307–317. http://dx.doi.org/10.1042/BJ20070209

Jan, Y.N., and L.Y. Jan. 2003. The control of dendrite development. *Neuron.* 40:229–242. http://dx.doi.org/10.1016/S0896-6273(03)00631-7

Jan, Y.N., and L.Y. Jan. 2010. Branching out: mechanisms of dendritic arborization. *Nat. Rev. Neurosci.* 11:316–328. http://dx.doi.org/10.1038/nrn2836

Lee, S.B., W. Kim, S. Lee, and J. Chung. 2007. Loss of LRRK2/PARK8 induces degeneration of dopaminergic neurons in *Drosophila*. *Biochem. Biophys. Res. Commun.* 358:534–539. http://dx.doi.org/10.1016/j.bbrc.2007.04.156

Lewis, P.A. 2009. The function of ROCO proteins in health and disease. *Biol. Cell.* 101:183–191. http://dx.doi.org/10.1042/BC20080053

Lin, C.H., P.I. Tsai, R.M. Wu, and C.T. Chien. 2010. *LRRK2* G2019S mutation induces dendrite degeneration through mislocalization and phosphorylation of tau by recruiting autoactivated GSK3β. *J. Neurosci.* 30:13138–13149. http://dx.doi.org/10.1523/JNEUROSCI.1737-10.2010

Lin, C.H., P.I. Tsai, R.M. Wu, and C.T. Chien. 2011. LRRK2 Parkinson's disease: from animal models to cellular mechanisms. *Rev. Neurosci.* 22:411–418. http://dx.doi.org/10.1515/rns.2011.036

Logarinho, E., and C.E. Sunkel. 1998. The *Drosophila* POLO kinase localises to multiple compartments of the mitotic apparatus and is required for the phosphorylation of MPM2 reactive epitopes. *J. Cell Sci.* 111:2897–2909.

MacLeod, D., J. Dowman, R. Hammond, T. Leete, K. Inoue, and A. Abeliovich. 2006. The familial Parkinsonism gene LRRK2 regulates neurite process morphology. *Neuron.* 52:587–593. http://dx.doi.org/10.1016/j.neuron.2006.10.008

MacLeod, D.A., H. Rhinn, T. Kuwahara, A. Zolin, G. Di Paolo, B.D. McCabe, K.S. Marder, L.S. Honig, L.N. Clark, S.A. Small, and A. Abeliovich. 2013. *RAB7L1* interacts with *LRRK2* to modify intraneuronal protein sorting and Parkinson's disease risk. *Neuron.* 77:425–439. (published erratum appears in *Neuron*. 2013. 77:994) http://dx.doi.org/10.1016/j.neuron.2012.11.033

Matanis, T., A. Akhmanova, P. Wulf, E. Del Nery, T. Weide, T. Stepanova, N. Galjart, F. Grosveld, B. Goud, C.I. De Zeeuw, et al. 2002. Bicaudal-D regulates COPI-independent Golgi–ER transport by recruiting the dynein–dynactin motor complex. *Nat. Cell Biol.* 4:986–992. http://dx.doi.org/10.1038/ncb891

Munro, S. 2011. The golgin coiled-coil proteins of the Golgi apparatus. *Cold Spring Harb. Perspect. Biol.* 3:3. http://dx.doi.org/10.1101/cshperspect.a005256

Ori-McKenney, K.M., L.Y. Jan, and Y.N. Jan. 2012. Golgi outposts shape dendrite morphology by functioning as sites of acentrosomal microtubule nucleation in neurons. *Neuron.* 76:921–930. http://dx.doi.org/10.1016/j.neuron.2012.10.008

Papoulas, O., T.S. Hays, and J.C. Sisson. 2005. The golgin Lava lamp mediates dynein-based Golgi movements during *Drosophila* cellularization. *Nat. Cell Biol.* 7:612–618. http://dx.doi.org/10.1038/ncb1264

Pierce, J.P., T. Mayer, and J.B. McCarthy. 2001. Evidence for a satellite secretory pathway in neuronal dendritic spines. *Curr. Biol.* 11:351–355. http://dx.doi.org/10.1016/S0960-9822(01)00077-X

Pulipparacharuvil, S., M.A. Akbar, S. Ray, E.A. Sevrioukov, A.S. Haberman, J. Rohrer, and H. Krämer. 2005. *Drosophila* Vps16A is required for trafficking to lysosomes and biogenesis of pigment granules. *J. Cell Sci.* 118:3663–3673. http://dx.doi.org/10.1242/jcs.02502

Rolls, M.M., D. Satoh, P.J. Clyne, A.L. Henner, T. Uemura, and C.Q. Doe. 2007. Polarity and intracellular compartmentalization of *Drosophila* neurons. *Neural Dev.* 2:7. http://dx.doi.org/10.1186/1749-8104-2-7

Sakaguchi-Nakashima, A., J.Y. Meir, Y. Jin, K. Matsumoto, and N. Hisamoto. 2007. LRK-1, a *C. elegans* PARK8-related kinase, regulates axonal-dendritic polarity of SV proteins. *Curr. Biol.* 17:592–598. http://dx.doi.org/10.1016/j.cub.2007.01.074

Satoh, D., D. Sato, T. Tsuyama, M. Saito, H. Ohkura, M.M. Rolls, F. Ishikawa, and T. Uemura. 2008. Spatial control of branching within dendritic arbors by dynein-dependent transport of Rab5-endosomes. *Nat. Cell Biol.* 10:1164–1171. http://dx.doi.org/10.1038/ncb1776

Scott, E.K., and L. Luo. 2001. How do dendrites take their shape? *Nat. Neurosci.* 4:359–365. http://dx.doi.org/10.1038/86006

Stafa, K., A. Trancikova, P.J. Webber, L. Glauser, A.B. West, and D.J. Moore. 2012. GTPase activity and neuronal toxicity of Parkinson's disease-associated LRRK2 is regulated by ArfGAP1. *PLoS Genet.* 8:e1002526.

Stone, M.C., F. Roegiers, and M.M. Rolls. 2008. Microtubules have opposite orientation in axons and dendrites of *Drosophila* neurons. *Mol. Biol. Cell.* 19:4122–4129. http://dx.doi.org/10.1091/mbc.E07-10-1079

Ultanir, S.K., N.T. Hertz, G. Li, W.P. Ge, A.L. Burlingame, S.J. Pleasure, K.M. Shokat, L.Y. Jan, and Y.N. Jan. 2012. Chemical genetic identification of NDR1/2 kinase substrates AAK1 and Rabin8 uncovers their roles in dendrite arborization and spine development. *Neuron.* 73:1127–1142. http://dx.doi.org/10.1016/j.neuron.2012.01.019

West, A.B., D.J. Moore, S. Biskup, A. Bugayenko, W.W. Smith, C.A. Ross, V.L. Dawson, and T.M. Dawson. 2005. Parkinson's disease-associated mutations in leucine-rich repeat kinase 2 augment kinase activity. *Proc. Natl. Acad. Sci. USA.* 102:16842–16847. http://dx.doi.org/10.1073/pnas.0507360102

Yadav, S., M.A. Puthenveedu, and A.D. Linstedt. 2012. Golgin160 recruits the dynein motor to position the Golgi apparatus. *Dev. Cell.* 23:153–165. http://dx.doi.org/10.1016/j.devcel.2012.05.023

Yang, W.K., Y.H. Peng, H. Li, H.C. Lin, Y.C. Lin, T.T. Lai, H. Suo, C.H. Wang, W.H. Lin, C.Y. Ou, et al. 2011. Nak regulates localization of clathrin sites in higher-order dendrites to promote local dendrite growth. *Neuron.* 72:285–299. http://dx.doi.org/10.1016/j.neuron.2011.08.028

Ye, B., Y. Zhang, W. Song, S.H. Younger, L.Y. Jan, and Y.N. Jan. 2007. Growing dendrites and axons differ in their reliance on the secretory pathway. *Cell.* 130:717–729. http://dx.doi.org/10.1016/j.cell.2007.06.032

Zheng, Y., J. Wildonger, B. Ye, Y. Zhang, A. Kita, S.H. Younger, S. Zimmerman, L.Y. Jan, and Y.N. Jan. 2008. Dynein is required for polarized dendritic transport and uniform microtubule orientation in axons. *Nat. Cell Biol.* 10:1172–1180. http://dx.doi.org/10.1038/ncb1777

Zhou, W., J. Chang, X. Wang, M.G. Savelieff, Y. Zhao, S. Ke, and B. Ye. 2014. GM130 is required for compartmental organization of dendritic Golgi outposts. *Curr. Biol.* 24:1227–1233. http://dx.doi.org/10.1016/j.cub.2014.04.008